Materials Advances

ROYAL SOCIETY OF CHEMISTRY

PAPER

View Article Online
View Journal | View Issue

Cite this: *Mater. Adv.*, 2025, 6, 2579

Equilibrium adsorption behaviour of a 3D-printed zeolite–geopolymer composite with high faujasitic content†

Carlo Gravino,[a] Nicola Gargiulo, *[b] Antonio Peluso,[a] Paolo Aprea,[a] Marco D'Agostini, [c] Giorgia Franchin, [c] Paolo Colombo [cde] and Domenico Caputo[abef]

In this work, a NaX zeolite/Na-activated geopolymer composite material having a 70 wt% zeolitic content was used for fabricating 3D-printed monoliths by means of Direct Ink Writing. The produced material was characterized employing X-ray diffraction, scanning electron microscopy and gas adsorption porosimetry, confirming that the NaX zeolite substantially retained its structure and properties after being mixed with the geopolymer matrix and undergoing the 3D printing process. In particular, the textural properties, specifically the specific surface area (242 $m^2\ g^{-1}$) and total pore volume (0.100 $cm^3\ g^{-1}$), exceed those already reported for comparable composites. CO_2 and water vapour adsorption isotherms of the samples were gravimetrically evaluated at 298.15, 318.15 and 338.15 K. CO_2 adsorption results (*e.g.*, about 3.2 mol kg^{-1} at 100 kPa and 298.15 K) suggested that, inside the composite, the NaX zeolite is the only active adsorbent for this adsorbate. On the other hand, water vapour adsorption results (*e.g.*, about 10.1 mol kg^{-1} at saturation and 298.15 K) showed that the geopolymer matrix was a significantly active adsorbent, working alongside the embedded NaX powders. The experimental data regarding both CO_2 and water vapour adsorption were well fitted by the semi-empirical Toth model, thus allowing determination of the respective isosteric heats of adsorption, with values significantly lower than those of pristine NaX powders. In the case of CO_2 adsorption, this is a positive finding in the light of possibly implementing this material in adsorption-based CO_2 capture technologies. Conversely, the same result for water vapour adsorption renders the material unsuitable for use in thermal energy storage devices.

Received 24th October 2024,
Accepted 1st March 2025

DOI: 10.1039/d4ma01074d

rsc.li/materials-advances

Introduction

Mitigating the effects of climate change caused by high emissions of greenhouse gases is one of the greatest challenges of our times.[1] To achieve this, an integrated approach is needed. On one hand, it is necessary to limit energy applications based on fossil fuels or increase their efficiency to reduce the formation of climate-altering emissions; on the other hand, it is necessary to limit CO_2 emissions into the environment through strategies for capturing the gas produced by widespread industrial processes. One of the most important technologies to remove CO_2 is adsorption. As an alternative CO_2 capture technology, adsorption using a variety of materials capable of reversibly or permanently removing CO_2 has been proposed as a viable approach with low energy requirements. A wide variety of adsorbents were investigated for CO_2 capture including carbons, silica, basic oxides, clays, zeolites, amine-containing porous materials, metal–organic frameworks (MOFs) and covalent organic frameworks (COFs).[2]

Therefore, it appears increasingly clear that applications of environmental interest are closely related to those of energy interest and *vice versa*. One of the latter ones is undoubtedly the storage of thermal energy in materials capable of reversibly releasing it by means of adsorption/desorption processes.[3] Usually, water vapour is considered the *de facto* standard adsorbate for this kind of technology.

[a] *Department of Chemical, Materials and Industrial Production Engineering, University of Naples Federico II, Piazzale Vincenzo Tecchio 80, 80125 Napoli, Italy*
[b] *Centre of Advanced Measurement and Technology Services (CeSMA), University of Naples Federico II, Corso N. Protopisani, 80146 Napoli, Italy. E-mail: ngargiul@unina.it*
[c] *Department of Industrial Engineering, University of Padua, Via Marzolo 9, 35131 Padova, Italy*
[d] *Department of Materials Science and Engineering, The Pennsylvania State University, University Park, PA 16802, USA*
[e] *National Interuniversity Consortium of Materials Science and Technology (INSTM), Via G. Giusti 9, 50121, Firenze, Italy*
[f] *CNR-STEMS Science and Technology for Sustainable Energy and Mobility, Via G. Marconi 4, 80125, Napoli, Italy*

† Electronic supplementary information (ESI) available. See DOI: https://doi.org/10.1039/d4ma01074d

As regards adsorbent materials, a specific synthetic type of faujasite mineral group – *i.e.*, the NaX zeolite – is well known for both its CO_2 and water vapour adsorption capabilities. Unfortunately, its conventional synthesis routes yield micrometric powders that pose problems related to their handling and would cause a significant pressure drop in powder-loaded fixed-bed columns. Because of these problems, it becomes necessary to appropriately shape zeolite powders. Recently, Papa *et al.* added NaX to a geopolymer slurry obtaining a zeolite–geopolymer composite suitable for the fabrication of monoliths.[4] Geopolymer slurries are obtained by combining aluminosilicate sources with an activating alkaline solution (generally based on sodium and/or potassium hydroxides or silicates of these alkaline metals). During the mixing phase, additives can be used (porous fillers, sacrificial fillers, chemical foaming agents, viscosity regulators, and reinforcing fibres) to modulate properties such as porosity, workability, setting time, thermal stability, thermal and electrical conductivity, and mechanical strength.[5,6] The already cited zeolite–geopolymer composite monoliths[4] show a relatively low NaX, *i.e.*, main adsorbent phase content (not more than 27.3 wt%) and, being fabricated by simple casting, would paradoxically cause the same issues associated with the use of loose powders when loaded into a fixed-bed column. Indeed, it is well known that the optimal performance of a monolithic mass transfer device is achieved when the device is fabricated with an open cell structure.[7]

For the latter reasons, the aim of this work is the fabrication of a monolithic adsorbent with an open cell structure made of a zeolite–geopolymer composite material. A NaX zeolite/Na-activated geopolymer composite having a 70 wt% zeolitic content was used for this purpose, and the open cell-structured monoliths were 3D-printed by means of Direct Ink Writing (DIW). Indeed, such an Additive Manufacturing technique allows for the fabrication of intricate, bespoke 3D structures that would be difficult to achieve through traditional manufacturing methods.[8] Moreover, the rheological properties of geopolymer-based inks can be tailored to enable precise deposition and shape retention during the printing process. The composite material produced in this work was preliminarily characterized using X-ray diffraction, scanning electron microscopy, gas adsorption porosimetry, He pycnometry, and mechanical testing. Subsequently, CO_2 and water vapour adsorption isotherms on the samples were gravimetrically evaluated at 298.15, 318.15, and 338.15 K, and the corresponding experimental data were modelled by the Toth semi-empirical equation for determining the isosteric heats of adsorption and other relevant parameters such as adsorbate affinities and maximum adsorption capacities.

Experimental

Adsorbent preparation

Alkaline solutions for the conversion of metakaolin to geopolymers were prepared by dissolving sodium silicate (SS2942, Ingessil, Italy) and NaOH pellets (reagent grade, Sigma-Aldrich, USA) in deionized water. The solution was left overnight to fully depolymerize. When considered together with the metakaolin, the amount of alkaline solution relative to metakaolin was selected to produce geopolymer slurries with an overall molar composition of 3.8 SiO_2: Al_2O_3: Na_2O: 18 H_2O.

DIW slurries were prepared by initially mixing the alkaline solution by means of a mechanical stand mixer (AM 20-D, Argolab, Italy) at a low speed (100 rpm). Zeolite NaX powder (Carlo Erba Reagenti, Italy) and Na-bentonite (ClearOFF Minerals, UK) as a rheological additive were added to the solution, and the mixing speed increased to 2200 rpm. Additional deionized water was required to compensate for the severe increase in viscosity caused by the introduction of the highly hydrophilic NaX filler, bringing the overall liquid-to-solid ratio of the slurry to 0.8 by mass. After 15 min of mixing at 2200 rpm, metakaolin (Argical 1200S, Imerys, France) was added as an aluminosilicate source for the geopolymer binder and the slurry was further mixed for 15 min at the same speed. Polycondensation of the geopolymer network yields a progressive increase in viscosity that can rapidly make a slurry unprintable; thus, in order to delay this phenomenon and increase the duration of the printing window, metakaolin was introduced last into the slurry and the temperature was held at 273.15 K during the entire mixing process by means of an ice bath.

The resulting slurry was placed into a 30cc syringe (Vieweg, Germany) for DIW. In a simplified overview of the process, the syringe is loaded onto a Delta-type 3D-printer (Delta 2040Turbo, WASP, Italy); the slurry is then pushed by compressed air from the syringe into the chamber of an auger extruder (LDM Extruder, WASP, Italy), from where it is finally extruded onto the build platform through a 0.84 mm tapered nozzle (Vieweg, Germany) by the mechanical action of the screw. In order to obtain prints of good quality with this technique, the rheology of the slurry must be tailored through the use of appropriate additives (Na-bentonite in the case of this work) to exhibit a pseudoplastic behavior and a yield stress for flow. The former facilitates extrusion through the nozzle when pressure is applied and allows shape retention through a rapid recovery of viscosity after deposition. Conversely, a sufficiently high yield strength allows the slurry to behave like an elastic solid when at rest, ensuring that the printed part does not collapse under its own weight. This is critical because, unlike other extrusion-based Additive Manufacturing technologies such as fused filament fabrication (FFF), the feedstock material in DIW does not immediately solidify during printing, necessitating a successive consolidation step such as drying or curing. Through this mechanism, the mobile printhead can shape the desired object layer by layer following a suitable pre-programmed print-path. Cylindrical samples with a log-pile scaffold geometry and 50% design porosity (labelled "3DZGC") composed of twelve 0.6 mm layers (overall dimensions Ø20xH7.2 mm) were produced in this manner.

After DIW, the 3DZGC samples were cured at 348.15 K and 100% Relative Humidity (RH) for 3 days, and subsequently dried at 348.15 K for 3 more days. After consolidation and drying, the final composites consisted of 70 wt% zeolite NaX, 27 wt% Na-geopolymer matrix with a molar composition of 3.8 SiO_2:Al_2O_3:Na_2O, and 3 wt% Na-bentonite.

Characterization methods

The X-ray diffraction (XRD) patterns of finely ground 3D-printed composite samples were acquired using a PANalytical X'Pert PRO apparatus with CuKα working radiation.

Morphological and microstructural analyses were performed by means of a Tescan Vega 4 scanning electron microscope (SEM). Observed monolithic samples were preliminarily gold-sputtered using a Cressington 108 coater.

The specific surface area (SSA) and porosity were analysed using N_2 adsorption at 77 K with a Micromeritics ASAP 2020 instrument. Samples crushed to macroscopic fragments were degassed at 473.15 K for 8 h. The SSA was evaluated using the Brunauer–Emmett–Teller (BET) model and following the recommendations by Rouquerol *et al.*[9] The total pore volume was estimated by applying the Gurvitch rule at $p/p_0 = 0.9$, while the micropore area and volume (together with the external surface area) were obtained by the *t*-plot method.

The bulk density (ρ_B) was calculated from the mass and external volume of the cylindrical 3DZGC samples. Apparent (ρ_A) and true densities (ρ_T) were measured using He pycnometry with an Anton Paar Ultrapyc 3000 on 3DZGC samples milled into macroscopic fragments ($d \approx 1$–5 mm) and fine powder ($d < 125$ μm), respectively. Open (P_O) and total porosities (P_T) were then computed from the three density values using eqn (1) and (2), respectively:

$$P_O = 1 - \frac{\rho_B}{\rho_A} \quad (1)$$

$$P_T = 1 - \frac{\rho_B}{\rho_T} \quad (2)$$

Mechanical testing was carried out on a Quasar 25 Universal Testing Machine (Galdabini, Italy). The samples were loaded in compression along the axis of the cylinder at a constant 0.5 mm min^{-1} rate until fracture, and the average value was taken as the compressive strength (σ_R).

CO_2 and water vapour adsorption measurements

CO_2 and water vapour adsorption isotherms were measured at three temperatures (298.15, 318.15, and 338.15 K) using a gravimetric apparatus with a McBain-type balance. A small platinum pan attached to a lab-made, gold-coated tungsten spring was pre-loaded with several milligrams of the crushed adsorbent sample. The CO_2 or water vapour adsorbed amount was indirectly determined by measuring the spring elongation due to the mass increase of the sample inside the pan. The extent of such elongation was obtained by using a cathetometer. Inside the adsorption chamber, pressure values were collected by means of an Edwards Datametrics 1500 capacitive transducer, while a FALC FA90 thermostatic control unit was used for keeping the temperature constant. Detailed schematics of the employed apparatus can be found elsewhere.[10] Before starting adsorption runs, the zeolite–geopolymer composite was degassed *in situ* at 473.15 K under high vacuum using an Edwards turbomolecular pump and a toroidal furnace. Each isothermal dataset was collected in triplicate.

Results and discussion

Characterization results

The Direct Ink Writing process allowed us to obtain porous, self-supporting monoliths like the one shown in Fig. 1.

Conventional cameras can easily show how these structured objects are composed of continuous filaments of regular size, deposited sequentially at orientations switching from 0 to 90° forming a porous 3D network.

Fig. 2 shows the XRD pattern of the ground zeolite–geopolymer composite along with the theoretical pattern of the hydrated NaX zeolite.

Except for minor differences in scale, the experimental pattern in Fig. 2 closely matches the theoretical pattern of the zeolitic

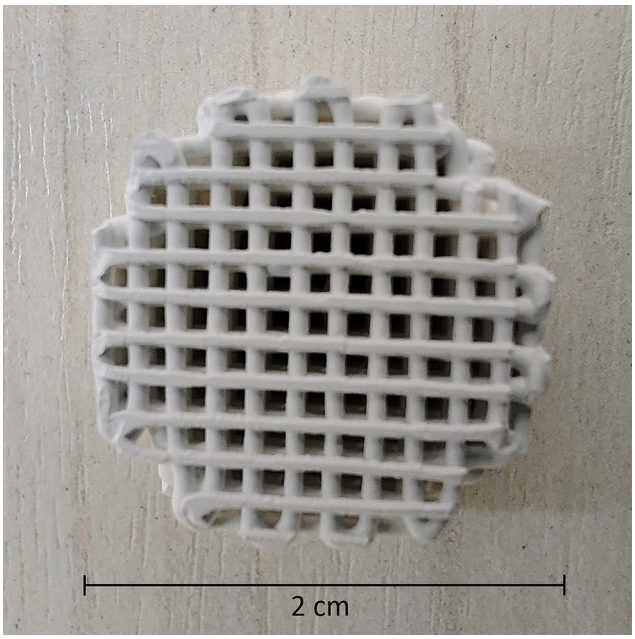

Fig. 1 Conventional photograph of a NaX-rich, 3D-printed zeolite–geopolymer composite sample.

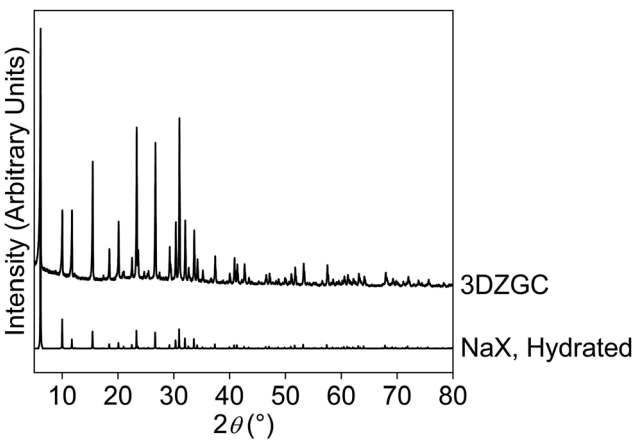

Fig. 2 XRD patterns of the ground NaX-rich, 3D-printed zeolite–geopolymer composite (experimental) and hydrated NaX zeolite (theoretical).

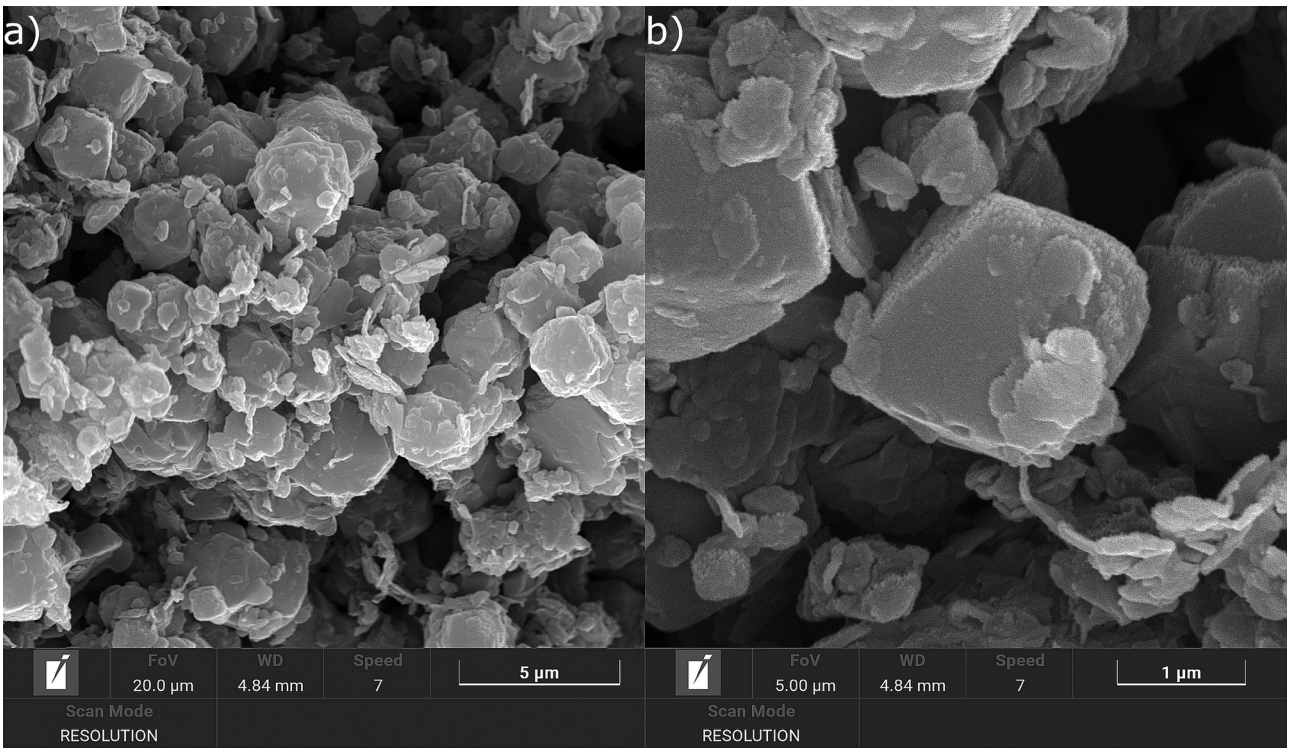

Fig. 3 SEM micrographs of the NaX-rich, 3D-printed zeolite–geopolymer composite.

phase in the composite sample. The experimental pattern in Fig. 2 does not show any diffraction characteristics of the geopolymer phase. Geopolymers typically exhibit a broad, glass-like hump between 20° and 35° 2ϑ, along with well-resolved peaks corresponding to impurities in the metakaolin.[11] The absence of any sign of the geopolymer in the pattern of 3DZGC is attributed to its low concentration, similar to observations in zeolite-rich tuffs with approximately 30 wt% volcanic glass.[12] The experimental pattern in Fig. 2 was also processed using the "Search & Match" feature of the X'Pert HighScore® suite, finding no other crystalline phase besides the NaX zeolite. These results are explained by the much higher concentration of the zeolite compared to that of the geopolymer matrix and the lack of significant impurities in the metakaolin.

Fig. 3 shows SEM micrographs of the NaX-rich, 3D-printed zeolite–geopolymer composite. As expected, the main morphology that is identifiable from the observation of the sample struts corresponds to the typical multifaceted/rhomboidal NaX zeolite crystals. The normal sharp edges of these crystals are somewhat rounded due to the interactions with the highly alkaline geopolymer matrix.[4] Although the geopolymer/zeolite ratio was quite low, the geopolymer matrix can still be seen as scattered, flaky particles around the zeolite crystals.

Fig. 4 shows the N_2 adsorption/desorption isotherm at 77 K of the NaX-rich, 3D-printed zeolite–geopolymer composite.

This isotherm is primarily of IUPAC type I, but shows two deviations from the typical form:

The slight increase in adsorption at $p/p_0 > 0.9$, which indicates some adsorption on the external surfaces of the zeolite crystals and geopolymer particles.

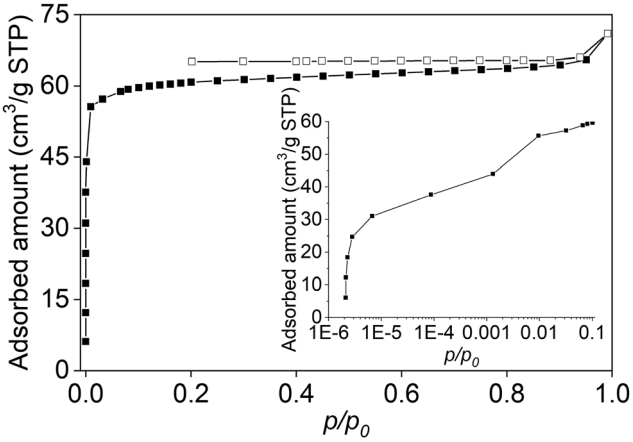

Fig. 4 N_2 adsorption (solid symbols)/desorption (open symbols) isotherm at 77 K of the NaX-rich, 3D-printed zeolite–geopolymer composite.

The low-pressure hysteresis, which is likely caused by the geopolymer reducing the size of some zeolite pores. This can worsen the gas diffusion limitations at low temperatures, which sometimes appear as discrepancies between the adsorption and desorption branches of the isotherm.[13]

The BET SSA of 3DZGC turned out to be 242 $m^2 g^{-1}$, 212 of which are related to the micropore surface according to *t*-plot results. Moreover, the *t*-plot micropore volume was found to measure 0.081 $cm^3 g^{-1}$, whereas the total pore volume obtained by applying the Gurvitch rule was 0.100 $cm^3 g^{-1}$. The textural properties of 3DZGC are all higher than those reported by Papa *et al.*[4], likely due to the higher zeolite content. In summary, the

results confirm that the NaX zeolite largely retained its structure and properties after mixing with the Na-activated geopolymer and 3D printing *via* Direct Ink Writing.

The total porosity of the 3DZGC scaffolds, measured by He pycnometry, was 68.11 ± 0.02%, significantly higher than the 50% design porosity introduced by the shaping process. This is attributed to the inherent micro- and macroporosity of the NaX zeolite and geopolymer matrix, respectively. Furthermore, the open porosity was 67.89 ± 0.02%, indicating good accessibility of the adsorption sites to the gas molecules.

The compressive strength was measured to be 0.59 ± 0.17 MPa. This low value is expected due to the high porosity and low geopolymer content. However, the loads from gas flow during operation are negligible. The monoliths need only to be strong enough for handling and installation, and this compressive strength is sufficient for these purposes.

Adsorption results

Fig. 5 presents the CO_2 and water vapour adsorption isotherms of the NaX-rich, 3D-printed zeolite–geopolymer composite at three different temperatures: 298.15, 318.15, and 338.15 K.

All isotherms display a distinct type I shape. The water vapour adsorption isotherms reach their respective saturation adsorbed amounts already at pressures around 1.5 kPa, as expected from an adsorbent primarily made of a low Si/Al ratio zeolite such as NaX. The noticeable scattering in all triplicate datasets suggests a degree of inhomogeneity in the adsorbent composition. Indeed, for every adsorption run, a different, very small portion of a printed monolith was removed and crushed before being loaded inside the balance.

For this reason, finding model isotherms that can provide information about the average behaviour of an adsorbent monolith becomes really important. To this end, the Toth isotherm[14] was chosen to model the experimental data in Fig. 5. The Toth isotherm is a semiempirical but quite thermodynamically consistent model: indeed, its equation can be reduced to Henry's law when approaching very low pressures, and it also shows a finite saturation limit when reaching significantly high pressures. Furthermore, its mathematical formulation does not include the saturation pressure of the adsorbate, making it suitable for modelling both subcritical and supercritical isotherms. At the same time, it contains a heterogeneity parameter whose optimized value can alternatively account for physical or chemical adsorption phenomena. According to this equation, the adsorptive pressure p and adsorbed amount q are related as follows:

$$q = q_{max}\frac{bp}{\left[1+(bp)^t\right]^{1/t}} \quad (3)$$

In eqn (3), q_{max}, b, and t are the model parameters. In particular, q_{max} symbolizes the saturation adsorption capacity, b is the affinity constant, and t is the aforementioned heterogeneity parameter, whose value is always positive but never higher than 1. Lower t values usually imply more heterogeneous (*i.e.*, chemisorption-like) processes. Indeed, for t = 1, the Toth isotherm becomes identical to the Langmuir isotherm, which describes particularly homogeneous (*i.e.*, "physi-like") adsorbent–adsorbate systems. As reported by Do,[15] the parameters in eqn (3) are usually temperature-dependent. As regards the affinity constant, its variability with temperature is governed by the following equation:

$$b = b_0 \exp\left[\frac{Q}{RT_0}\left(\frac{T_0}{T}-1\right)\right] \quad (4)$$

where b_0 is the value of b at a reference temperature T_0, R is the molar gas constant, and Q is a quantity related to the heat of adsorption. The temperature dependence of q_{max} can be expressed by the following empirical formula:

$$q_{max} = q_{max,0} \exp\left[\chi\left(1-\frac{T}{T_0}\right)\right] \quad (5)$$

where $q_{max,0}$ is the value of q_{max} at T_0 and χ is a dimensionless, non-negative parameter. The heterogeneity parameter can also vary with temperature;[15] however, in this study, this adjustment

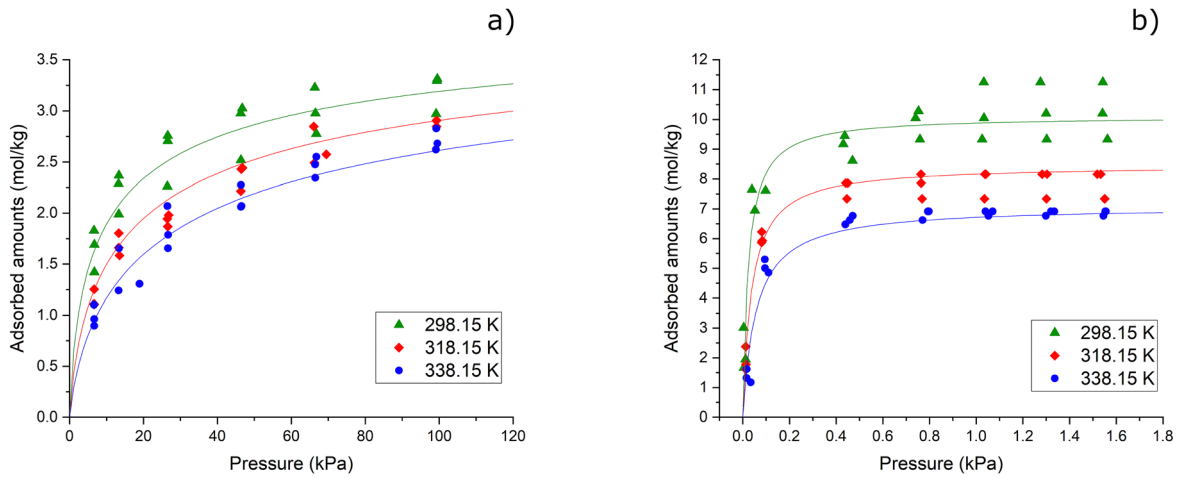

Fig. 5 CO_2 (a) and water vapour (b) adsorption isotherms (triplicate measurements) of the NaX-rich, 3D-printed zeolite–geopolymer composite at 298.15, 318.15 and 338.15 K. Continuous lines: best fitting Toth model isotherms.

Table 1 Toth parameters for CO_2 and water vapour adsorption on the NaX-rich, 3D-printed zeolite–geopolymer composite

	CO_2		H_2O vapour	
	Value	Standard error	Value	Standard error
$q_{max,0}$ (mol kg^{-1})	4.14833	0.52835	10.10605	0.22960
χ (dimensionless)	0 (fixed)	0	2.64049	0.26160
b_0 (kPa^{-1})	0.32787	0.13429	43.03692	10.7688
Q (kJ mol^{-1})	24.13960	2.24594	18.47563	5.23283
t (dimensionless)	0.53972	0.11814	1 (upper bound)	0.15955
	Coefficient of determination R^2 = 0.934		Coefficient of determination R^2 = 0.943	

did not significantly improve the data fitting quality. Therefore, t was kept constant with temperature to simplify model implementation. Indeed, eqn (3)–(5) were coded inside the Origin Pro® environment using the Fitting Function Organizer tool, and then the experimental data in Fig. 5 were submitted to nonlinear regression for simultaneously computing the optimal values of b_0, Q, t, $q_{max,0}$ and χ. The best-fit values of these parameters, calculated using T_0 = 298.15 K, are shown in Table 1, and the graphical comparison between the model and experimental results can be seen in Fig. 5, where the symbols pertain to the experimental measurements and the continuous curves refer to the best-fit Toth model isotherms.

Regarding CO_2 adsorption isotherms, incorporating the temperature dependence of q_{max} did not enhance the data fitting quality. This suggests that the CO_2 saturation adsorption capacity of the NaX-rich, 3D-printed zeolite–geopolymer composite is temperature-independent. For this reason, the value of χ was fixed equal to zero when modelling the CO_2 adsorption isotherms. On the other hand, fitting water vapour adsorption data led the heterogeneity parameter to converge towards the unit value, thus reducing the resulting model isotherms to typical Langmuir curves. The latter observation can be usually expected for water vapour adsorption on zeolites, which is a process characterized by quite a high adsorbent–adsorbate affinity while, however, preserving an essentially physisorption-like behaviour.

Regarding the adsorption modelling results, the key observations are as follows:

(1) The ambient temperature value of the affinity coefficient b for CO_2 adsorption is in line with values reported in the literature for NaX powders,[16] which in turn are significantly lower than those relating to monolithic adsorbents that rely on reversible chemisorption processes;[17]

(2) The value of the heterogeneity parameter t for CO_2 adsorption is significantly lower than 1 and, again, in line with values reported for NaX powders,[16] confirming how CO_2 adsorption on NaX develops through specific interactions, which were found to produce carbonate-like species starting from basic framework oxygen atoms and CO_2 molecules polarized on neighbouring Na^+ ions.[18]

Once model curves that average the adsorption behaviour of the fabricated monoliths were obtained, a comparison at 298.15 K was carried out with both CO_2 and water vapour experimental adsorption isotherms of the pristine NaX powder used for preparing the 3D-printing ink (Fig. 6).

In Fig. 6, the CO_2 adsorption data were collected specifically for this study, whereas the water vapour adsorption data on the same adsorbent were sourced from the literature.[19] Fig. 6(a) clearly shows the difference between the equilibrium adsorption capacities of pristine NaX powders and the fabricated composite. Unlike previous reports,[4] the geopolymer binder used in this study does not contain any additional zeolitic phase capable of contributing to CO_2 adsorption. Considering, for example, the CO_2 adsorbed amounts at 100 kPa and 298.15 K, the corresponding estimated values from Fig. 6(a)

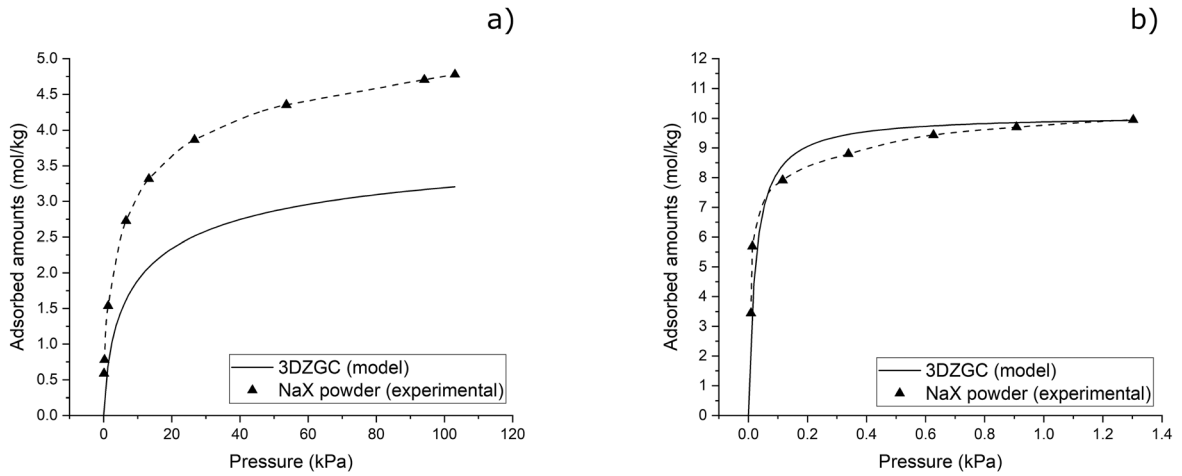

Fig. 6 Comparison between the model CO_2 (a) and water vapour (b) adsorption isotherms of the NaX-rich, 3D-printed zeolite–geopolymer composite and the corresponding experimental isotherms of pristine NaX powders at 298.15 K.

for 3DZGC and pristine NaX powders are 3.2 and 4.7 mol kg^{-1}, respectively. The ratio among these quantities is about 0.7, *i.e.*, the actual content of NaX powders inside 3DZGC. A completely different scenario arises from the analysis of Fig. 6(b), where the shown isotherms are almost superimposable. Indeed, totally amorphous, sodium-activated geopolymers can adsorb significant water vapour amounts.[20] Therefore, the specific water vapour adsorption capacity of the geopolymer binder inside 3DZGC is most probably comparable to, if not higher than that of the NaX zeolite, thus leading to the peculiar result shown in Fig. 6(b).

The previously described modelling approach was also useful for investigating the isosteric heat of adsorption for both adsorbates. Indeed, having information about the isosteric heat of CO_2 adsorption is crucial for designing pressure swing adsorption (PSA) and temperature swing adsorption (TSA) fixed beds, which essentially work in an adiabatic way. As regards water vapour, the knowledge of the isosteric heat of adsorption represents the first step for calculating parameters, such as the specific heat storage density, which are essential for evaluating the use of a specific adsorbent inside thermal energy storage devices. The isosteric heat of adsorption (ΔH) can be calculated from the van't Hoff equation:[15]

$$\frac{\Delta H}{RT^2} = -\left(\frac{\partial \ln p}{\partial T}\right)_q \quad (6)$$

A general expression for ΔH as a function of the fractional coverage $\theta = q/q_{max}$ can be derived by rewriting eqn (3) in terms of *p versus q*, substituting eqn (4) and (5) and differentiating its natural logarithm with respect to *T*. However, for CO_2 adsorption on 3DZGC, this procedure is significantly simplified as q_{max} is temperature-independent. As a result, the isosteric heat of CO_2 adsorption on 3DZGC is independent of θ and its modulus is equal to *Q*. Such a value is significantly lower than that of others similarly obtained for CO_2 adsorption on NaX powders.[21,22] As already mentioned, fixed-bed adsorption is a substantially adiabatic operation, so the isosteric heat of adsorption causes temperature increases during the process. Once the working conditions are set, because the adsorption capacity decreases with increasing temperature, the adsorbent materials used in fixed beds are thus systematically prone to losing part of their adsorption capacity as the working temperature rises. Therefore, given the adsorptive to be captured, a lower isosteric heat of adsorption is desirable when choosing the corresponding adsorbent. As regards water vapour adsorption on 3DZGC, the already described procedure for obtaining an analytical form of ΔH can be simplified by substituting eqn (3) with the Langmuir equation due to the fitting results reported in Table 1. The resulting function has already been derived elsewhere[23] and takes the following form:

$$-\Delta H = Q + \frac{\chi RT^2}{T_0}\frac{1}{1-\theta} \quad (7)$$

The parametric relationship between $\Delta H(\theta)$ and *T* makes eqn (7) substantially useless for calculating useful physical quantities such as the specific heat storage density. Consequently, the isosteric heat of water vapour adsorption on 3DZGC was numerically obtained as a function of *q* by linear regression of selected isosteres (Fig. 7).[19] In this procedure, the inverse function of the model isotherms in Fig. 5(b) was used for easily calculating the (*T*, *p*) couples to be charted on the isostere plot.

Analysing Fig. 7(a) reveals how the opposite of the isosteric heat increases while approaching the adsorbent saturation capacity, which is a common behaviour when adsorbing condensable vapours and q_{max} depend on the temperature.[23,24] Surprisingly, the values of $-\Delta H$ reported in Fig. 7(a) are much lower than most of the others that can be found in the literature for water vapour adsorption on NaX powders.[19,25–27]

The specific heat storage density (ΔH_{int}), *i.e.*, one of the main parameters for evaluating the eligibility of an adsorbent inside a thermal energy storage device, is defined as follows:[19]

$$\Delta H_{int} = \int_{q_{d\text{-phase}}}^{q_{a\text{-phase}}} \Delta H \mathrm{d}q \quad (8)$$

In eqn (8), $q_{d\text{-phase}}$ and $q_{a\text{-phase}}$ are the amounts of water vapour retained by the adsorbent at the end of desorption and adsorption phases of the thermodynamic cycle, respectively. Keeping in mind that the values of the isosteric heat of water vapour

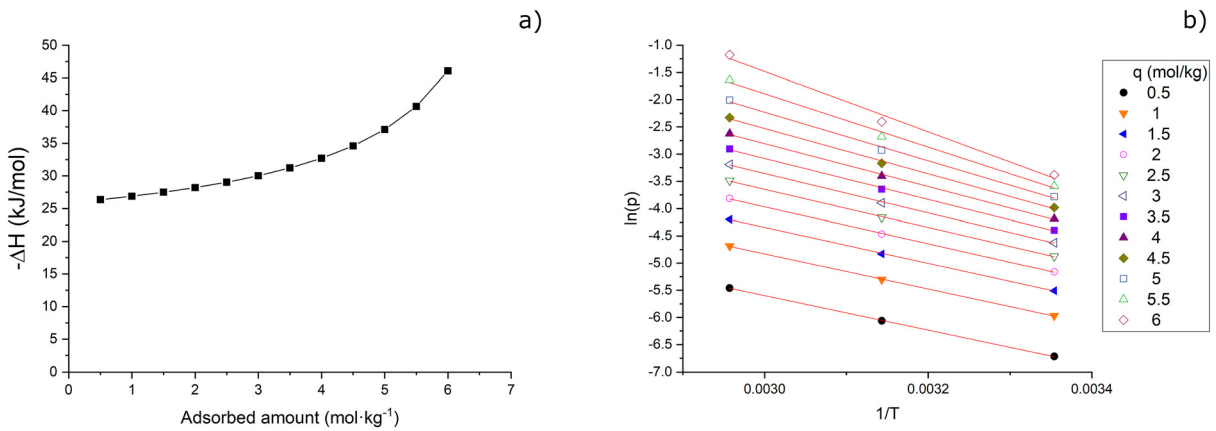

Fig. 7 Isosteric heat of water vapour adsorption on the NaX-rich, 3D-printed zeolite–geopolymer composite (a) and the corresponding isostere plot (b).

adsorption on NaX powders can be already considered sub-par for obtaining good heat storage densities,[19,28] the results shown in Fig. 7 suggest that 3DZGC is not a good adsorbent for designing thermal energy storage devices.

Conclusions

Using an Additive Manufacturing approach based on the Direct Ink Writing technology, we successfully fabricated a 3D-structured monolithic adsorbent that incorporates an unprecedented 70 wt% of commercial NaX zeolite powders inside a geopolymer matrix and offers both mechanical stability and hierarchical porosity. The X-ray diffraction pattern of the produced composite material showed an impressive overlap with the pattern of the pristine NaX zeolite, thus revealing that no secondary crystalline phases formed within the geopolymer matrix and confirming the stability of the zeolite within the matrix. Furthermore, the textural properties (*e.g.*, specific surface area and total pore volume) are higher than those already reported for comparable composites. All the characterization results reported thus confirm that the NaX zeolite largely retained its structure and properties after being mixed with the Na-activated geopolymer matrix and undergoing 3D printing. Ultimately, the total porosity of the fabricated monoliths far exceeds the 50% design porosity introduced by the shaping process and their compressive strength appears adequate for routine handling and installation procedures in fixed-bed columns.

CO_2 equilibrium adsorption results suggested that the NaX zeolite was the only active adsorbent inside the composite. Indeed, a comparison between the CO_2 amounts adsorbed by the fabricated samples and pristine NaX powders yielded the same 0.7 ratio, corresponding to the NaX content inside the monoliths. Moreover, the Toth adsorption model parameters for the fabricated samples were quite comparable to those of pristine NaX powders. On the other hand, water vapour equilibrium adsorption results showed that the geopolymer matrix was a significantly active adsorbent together with the embedded NaX powders. Indeed, water vapour adsorption isotherms at ambient temperature for the fabricated samples and pristine NaX powders were almost superimposable.

Determining the isosteric heat of both CO_2 and water vapour adsorption on 3DZGC revealed that their values were significantly lower than those of pristine NaX powders. In the case of CO_2 adsorption, this is a positive finding in view of the potential implementation of the produced components in adsorption-based CO_2 capture technologies. In contrast, the same result for water vapour adsorption indicates that the material is not suitable for use in thermal energy storage devices. Further investigations are needed to assess the feasibility of packing pre-pilot columns with monoliths homologous to those fabricated in this work for effective CO_2 adsorption.

Author contributions

Conceptualization: N. G.; data curation: C. G and A. P.; formal analysis: N. G.; funding acquisition: P. C. and D. C.; investigation: C. G., A. P. and M. D.; methodology: G. F., P. C. and D. C.; project administration: P. C. and D. C.; resources: P. C. and D. C.; software: N. G.; supervision: G. F., P. C. and D. C.; validation: N. G., P. A., G. F., P. C. and D. C.; visualization: C. G., N. G., A. P., P. A., M. D., G. F., P. C. and D. C.; writing – original draft: C. G., N. G. and A. P.; writing – review and editing: P. A., G. F., P. C. and D. C.

Data availability

The data supporting this article have been included as part of the ESI.†

Conflicts of interest

There are no conflicts to declare.

Acknowledgements

The Italian Ministry of University and Research (PRIN2017 Grant Number 2017PMR932) supported this work.

References

1 K. J. Mach, K. Jagannathan, L. Shi, L. L. Turek-Hankins, J. R. Arnold, C. Brelsford, A. N. Flores, J. Gao, C. E. Martín, D. L. McCollum, R. Moss, J. Niemann, B. Rashleigh and P. M. Reed, *Earth Future*, 2024, **12**, e2023EF004392.
2 X. Y. D. Soo, J. J. C. Lee, W.-Y. Wu, L. Tao, C. Wang, Q. Zhu and J. Bu, *J. CO_2* Util., 2024, **81**, 102727.
3 C. Feng, E. Jiaqiang, W. Han, Y. Deng, B. Zhang, X. Zhao and D. Han, *Renewable Sustainable Energy Rev.*, 2021, **144**, 110954.
4 E. Papa, V. Medri, S. Amari, J. Manaud, P. Benito, A. Vaccari and E. Landi, *J. Clean. Prod.*, 2018, **171**, 76–84.
5 P. Rożek, M. Król and W. Mozgawa, *J. Clean. Prod.*, 2019, **230**, 557–579.
6 X. Zhang, C. Bai, Y. Qiao, X. Wang, D. Jia, H. Li and P. Colombo, *Compos. – A: Appl. Sci. Manuf.*, 2021, **150**, 106629.
7 F. Brandani, A. Rouse, S. Brandani and D. M. Ruthven, *Adsorption*, 2004, **10**, 99–109.
8 S. Ma, S. Fu, S. Zhao, P. He, G. Ma, M. Wang, D. Jia and Y. Zhou, *Addit. Manuf.*, 2021, **46**, 102202.
9 J. Rouquerol, P. Llewellyn and F. Rouquerol, in *Characterization of Porous Solids VII*, ed. P. Llewellyn, F. Rodriguez-Reinoso, J. Rouquerol and N. Seaton, Elsevier, 2007, pp. 49–56.
10 A. Macario, A. Katovic, G. Giordano, F. Iucolano and D. Caputo, *Microporous Mesoporous Mater.*, 2004, **81**, 139–147.
11 S. Dai, H. Wang, S. An and L. Yuan, *Materials*, 2022, **15**, 2957.
12 J. Garcia, M. Gonzalez, J. Caceres and J. Notario, *Zeolites*, 1992, **12**, 664–669.
13 T. Zelenka, L. Zelená, C. Abreu-Jaureguí, J. Silvestre-Albero, G. Zelenková and V. Slovák, *Small*, 2024, **20**, 2311990.
14 J. Toth, *Adv. Colloid Interface Sci.*, 1995, **55**, 1–239.

15 D. D. Do, *Adsorption Analysis: Equilibria and Kinetics*, Imperial College Press, London, 1998.
16 K. S. Walton, M. B. Abney and M. D. LeVan, *Microporous Mesoporous Mater.*, 2006, **91**, 78–84.
17 N. Gargiulo, A. Verlotta, A. Peluso, P. Aprea and D. Caputo, *Microporous Mesoporous Mater.*, 2015, **215**, 1–7.
18 G. Martra, S. Coluccia, P. Davit, E. Gianotti, L. Marchese, H. Tsuji and H. Hattori, *Res. Chem. Intermed.*, 1999, **25**, 77–93.
19 P. Aprea, B. de Gennaro, N. Gargiulo, A. Peluso, B. Liguori, F. Iucolano and D. Caputo, *Appl. Therm. Eng.*, 2016, **106**, 1217–1224.
20 X. Ke and V. A. Baki, *Microporous Mesoporous Mater.*, 2021, **325**, 111329.
21 P. Aprea, D. Caputo, N. Gargiulo, F. Iucolano and F. Pepe, *J. Chem. Eng. Data*, 2010, **55**, 3655–3661.
22 N. Gargiulo, K. Shibata, A. Peluso, P. Aprea, T. Valente, G. Pezzotti, T. Shiono and D. Caputo, *Int. J. Environ. Sci. Technol.*, 2018, **15**, 1543–1550.
23 N. Gargiulo, A. Peluso, P. Aprea, O. Marino, R. Cioffi, E. Jannelli, S. Cimino, L. Lisi and D. Caputo, *Renewable Energy*, 2019, **138**, 230–235.
24 N. Gargiulo, A. Peluso, P. Aprea, M. Eić and D. Caputo, *J. Colloid Interface Sci.*, 2019, **554**, 463–467.
25 N. M. Hassan, T. K. Ghosh, A. L. Hines and S. K. Loyalka, *Chem. Eng. Commun.*, 1991, **105**, 241–253.
26 A. Di Lella, N. Desbiens, A. Boutin, I. Demachy, P. Ungerer, J.-P. Bellat and A. H. Fuchs, *Phys. Chem. Chem. Phys.*, 2006, **8**, 5396–5406.
27 K. G. Wynnyk, B. Hojjati and R. A. Marriott, *Ind. Eng. Chem. Res.*, 2018, **57**, 15357–15365.
28 H. Stach, J. Mugele, J. Jänchen and E. Weiler, *Adsorption*, 2005, **11**, 393–404.